

## Coastal groundwater dynamics off Santa Barbara, California: Combining geochemical tracers, electromagnetic seepmeters, and electrical resistivity

Peter W. Swarzenski<sup>a,\*</sup>, John A. Izbicki<sup>b</sup>

<sup>a</sup>U.S. Geological Survey, Center for Coastal & Watershed Studies, 400 Natural Bridges Drive, Santa Cruz, CA 95060, USA

<sup>b</sup>U.S. Geological Survey, 4165 Spruance Road, Suite 200, San Diego, CA 92101, USA

### ARTICLE INFO

#### Article history:

Received 21 January 2009

Accepted 15 March 2009

Available online 5 April 2009

#### Keywords:

submarine groundwater discharge

radium

radon

electrical resistivity

nutrients

Santa Barbara

### ABSTRACT

This paper presents repeat field measurements of  $^{222}\text{Rn}$  and  $^{223,224,226,228}\text{Ra}$ , electromagnetic seepage meter-derived advective fluxes, and multi-electrode, stationary and continuous marine resistivity surveys collected between November 2005 and April 2007 to study coastal groundwater dynamics within a marine beach in Santa Barbara, California. The study provides insight into magnitude and dynamics of submarine groundwater discharge (SGD) and associated nutrient loadings into near-shore coastal waters, where the predominant SGD drivers can be both spatially and temporally separated. Rn-222 and  $^{223,224,226,228}\text{Ra}$  were utilized to quantify the total and saline contribution, respectively, of SGD. The two short-lived  $^{224,223}\text{Ra}$  isotopes provided an estimate of apparent near-shore water mass age, as well as an estimate of the Ra-derived eddy diffusion coefficient,  $K_h$  ( $^{224}\text{Ra} = 2.86 \pm 0.7 \text{ m}^2 \text{ s}^{-1}$ ;  $^{223}\text{Ra} = 1.32 \pm 0.5 \text{ m}^2 \text{ s}^{-1}$ ). Because  $^{222}\text{Rn}$  ( $t_{1/2} = 3.8 \text{ day}$ ) and  $^{224}\text{Ra}$  ( $t_{1/2} = 3.66 \text{ day}$ ) have comparable half-lives and production terms, they were used in concert to examine respective water column removal rates. Electromagnetic seepage meters recorded the physical, bi-directional exchange across the sediment/water interface, which ranged from  $-6.7$  to  $14.5 \text{ cm day}^{-1}$ , depending on the sampling period and position relative to the low tide line. Multi-day time-series  $^{222}\text{Rn}$  measurements in the near-shore water column yielded total (saline + fresh) SGD rates that ranged from  $3.1 \pm 2.6$  to  $9.2 \pm 0.8 \text{ cm day}^{-1}$ , depending on the sampling season. Offshore  $^{226}\text{Ra}$  ( $t_{1/2} = 1600 \text{ year}$ ) and  $^{222}\text{Rn}$  gradients were used with the calculated  $K_h$  values to determine seabed flux estimates ( $\text{dpm m}^{-2} \text{ day}^{-1}$ ), which were then converted into SGD rates ( $7.1$  and  $7.9 \text{ cm day}^{-1}$ , respectively). Lastly, SGD rates were used to calculate associated nutrient loads for the near-shore coastal waters off Santa Barbara. Depending on both the season and the SGD method utilized, the following SGD-derived nutrient inputs were computed ( $\text{mol per day per meter of shoreline}$ ):  $\text{NH}_4^+ = 0.06\text{--}0.29 \text{ mol day}^{-1} \text{ m}^{-1}$ ;  $\text{SiO}_4 = 0.22\text{--}0.29 \text{ mol day}^{-1} \text{ m}^{-1}$ ;  $\text{PO}_4^{3-} = 0.04\text{--}0.17 \text{ mol day}^{-1} \text{ m}^{-1}$ ;  $[\text{NO}_2^- + \text{NO}_3^-] = 0\text{--}0.52 \text{ mol day}^{-1} \text{ m}^{-1}$ ; dissolved inorganic nitrogen (DIN) =  $0.01\text{--}0.17 \text{ mol day}^{-1} \text{ m}^{-1}$ , and dissolved organic nitrogen (DON) =  $0.08\text{--}0.09 \text{ mol day}^{-1} \text{ m}^{-1}$ . Compared to the ephemeral nature of fluvial and marine inputs into this region, such SGD-derived loadings can provide a sustained source of select nutrients to the coastal waters off Santa Barbara, California that should be accounted for in mass balance estimates.

Published by Elsevier Ltd.

### 1. Introduction

It is now well accepted that submarine groundwater discharge (SGD), an almost ubiquitous coastal process, may substantially impact certain near-shore material budgets (Capone and Bautista, 1985; Moore, 2006; Burnett et al., 2006; Swarzenski, 2007; Charrette et al., 2008). While the contribution of SGD-derived nutrients, bacteria, carbon, and select trace elements such as Ba or U (Charette and Sholkovitz, 2006; Swarzenski and Baskaran, 2007) can vary

widely depending on both local hydrogeologic conditions and anthropogenic perturbations, accurate assessments of the spatial and temporal distribution of SGD along a particular coastline remain rare (Burnett et al., 2002; Dulaiova et al., 2006b). This paucity of reliable data stems in large part in that SGD remains the 'hidden' vector in water and material transport from land to the sea, and that the physical drivers of SGD are complex, often inter-related, and still poorly constrained (Taniguchi, 2002; Michael et al., 2005; Robinson et al., 2007a,b). Furthermore, the discharge of submarine groundwater is usually expressed not through well-defined marine springs (Swarzenski et al., 2001), but rather through diffuse discharge that is often ephemeral and patchy in nature (Burnett et al., 2002; Taniguchi et al., 2003).

\* Corresponding author.

E-mail address: [pswarzen@usgs.gov](mailto:pswarzen@usgs.gov) (P.W. Swarzenski).

Nonetheless, significant advances have recently been made in the application of select U/Th-series radionuclides as quantitative tracers of SGD (Moore, 1996, 2000a,b; Moore and de Oliveira, 2008; Burnett et al., 2001, 2002, 2003; Charette et al., 2001, 2008; Dulaiova and Burnett, 2004, 2006; Dulaiova et al., 2005, 2006a,b). Such tracer techniques can yield unprecedented information on: (i) SGD 'hotspots'; (ii) the source waters for SGD; (iii) the magnitude and dynamics of SGD rates; and (iv) the relative composition of SGD (i.e., fresh versus saline contributions). As proxies for fluid exchange these tracers are limited by how well they move with a mixed-salinity water parcel, and local quantification of fluid exchange is still most directly measured by some seepage meter device (Mulligan and Charette, 2006). Seepmeters, outfitted with autonomous salinity, temperature, and pressure sensors, can measure the bi-directional exchange of fluid across the sediment/water interface with high resolution (Taniguchi and Fukuo, 1993; Taniguchi et al., 2003, 2007). Such datasets can provide useful

constraints on the geochemical tracer-derived SGD results (Burnett et al., 2006; Swarzenski et al., 2007a). An additional complementary tool to study the movement of the fresh water/salt water interface and to map the geographic extent of a coastal SGD zone is stationary (land-based) electrical resistivity (Swarzenski et al., 2006a, 2007a,b; Taniguchi et al., 2007).

In environments that are fresh water limited or have low hydraulic gradients, the submarine exchange of groundwater often contains a large component of recycled sea water (Colbert and Hammond, 2007a,b; Colbert et al., 2008a,b; Weinstein et al., 2007). In such systems, even though the net discharge may be small or even negative (i.e., sea water infiltration), this continuous cycle of recharge and discharge, driven by waves and tides, may still significantly impact the flow of nutrients from land to the sea. In this paper, we address the exchange of groundwater with sea water at West Beach in Santa Barbara, California (Fig. 1), using a suite of geochemical tracers and electrical geophysical techniques. From

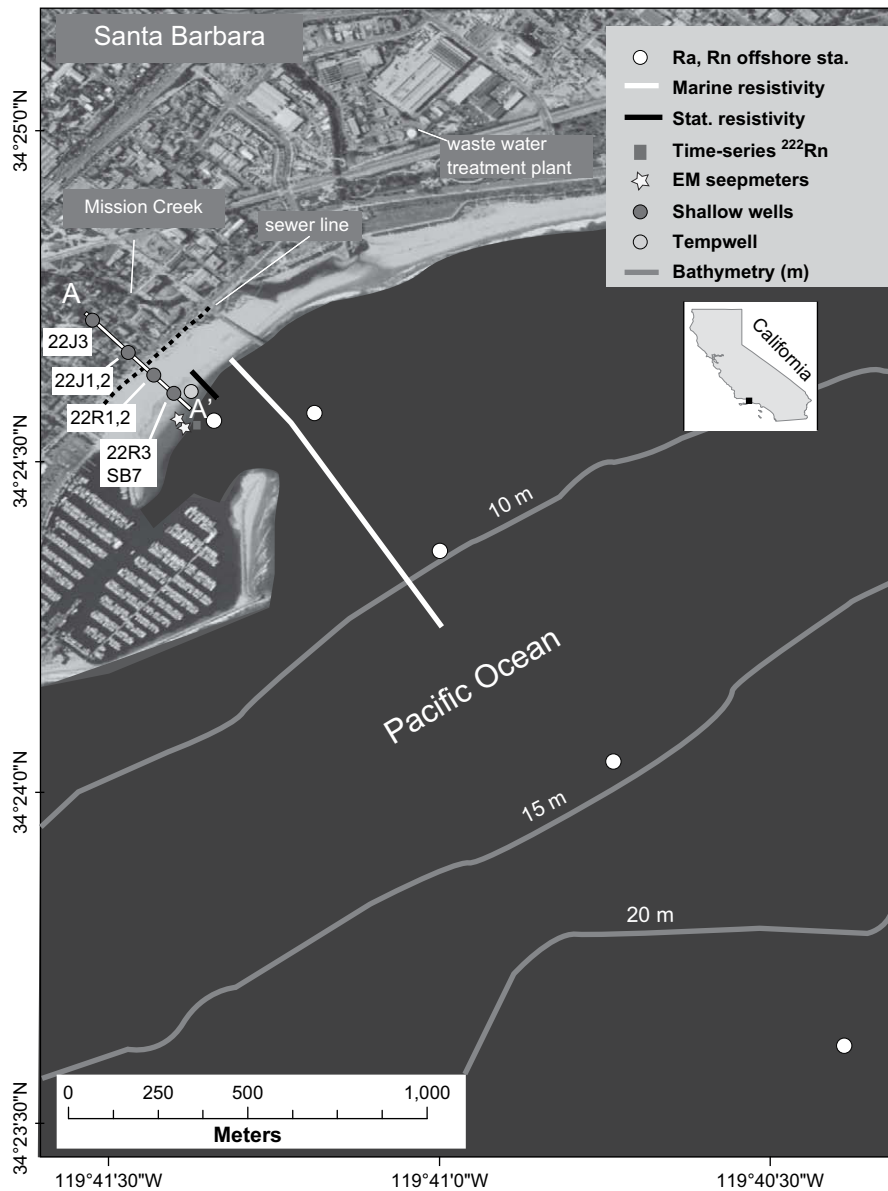


**Fig. 1.** West Beach, Santa Barbara, California showing the position of the electromagnetic seepmeters, time-series Rn deployments, offshore transect sites (Rn and Ra) and the streamer location for land-based, multi-electrode and the marine continuous resistivity profile. Also shown is the shore-parallel running sewer line (which may be a source of excess nutrients and bacteria to the beach), the nearby waste water treatment plant, and the position of the hydrogeologic transect (A–A') shown in Fig. 3.

calculated fluid exchange rates per season, we are able to derive SGD nutrient loading estimates. On the basis of our results, we have determined that the wave/tide-driven exchange of shallow groundwater with coastal sea water can convey a sustained load of select nutrients and trace elements to the near-shore waters off Santa Barbara, California, even without a net flow of fresh groundwater towards the sea.

**2. Study site**

Field data were collected at a meso-tidal, sandy beach ('West Beach') adjacent to Santa Barbara, California (Fig. 1), where fecal indicator bacteria (FIB) in the surf zone are occasionally present at high enough concentrations to necessitate beach warnings or closures (Izbicki et al., in review). Three beach and water column sampling campaigns targeted spring tide (November 2005, April

2007) and neap tide (May/June 2006) cycles, as well as seasonal variations (Fig. 2). Mission Creek, which discharges adjacent to West Beach, is an obvious potential source for FIB, as are subaerial and submarine groundwater discharge (Boehm et al., 2004; Paytan et al., 2004; Boehm and Weisberg, 2005; Boehm, 2007; Yamahara et al., 2007) and any possible leakage from the shore-parallel municipal sewer line that lies buried beneath the landward edge of West Beach. While a companion report addresses the various sources of FIB and their hydrologic forcing in coastal Santa Barbara (Izbicki et al., in review), here we examine the marine effects (i.e., tides) on groundwater exchange and associated nutrient loading to the coastal waters of Santa Barbara Harbor. Details on the hydro-geologic setting of this study site can be found in Muir (1968), Martin (1984), and Freckleton et al. (1998).

Santa Barbara, located about 150 km northwest of Los Angeles along the Pacific coast of the United States, has a Mediterranean-

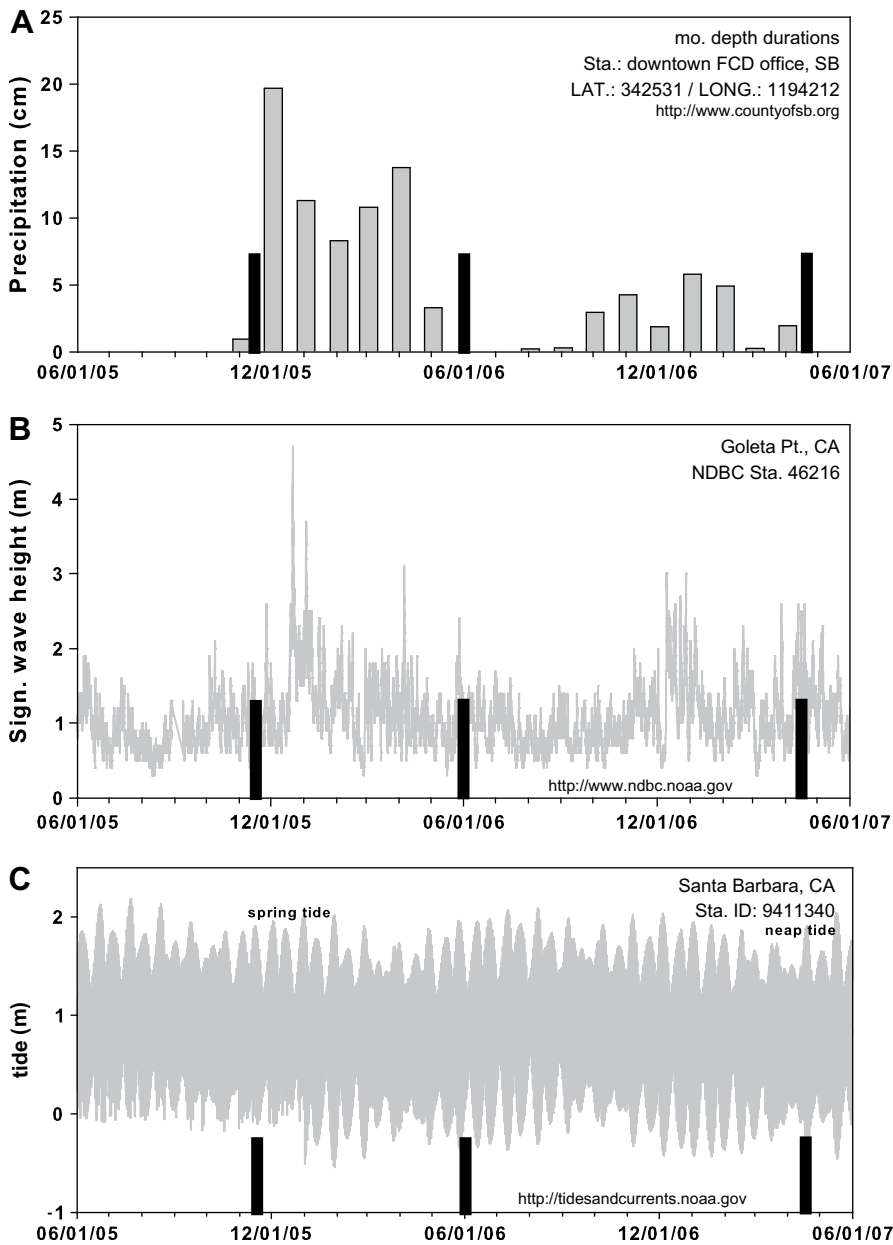


**Fig. 2.** Black bars denote sampling events as a function of: (A) the monthly precipitation record for down-town Santa Barbara, California; (B) significant wave height (m); and (C) the verified tide record (m) from 06/2005 to 06/2007. Sampling events were coordinated around maximum tides and seasons.

type climate characterized by relatively dry and mild summers and winter months that can be periodically cool and wet. Temperatures are moderated by the sea; mean winter temperatures are  $\sim 13^\circ\text{C}$ , while summer temperatures average  $18^\circ\text{C}$ . The population of Santa Barbara exceeded 90,000 in 2004 (<http://www.santabarbaraca.gov>) and is confined along a narrow ( $\sim 5$  km wide) but highly developed coastal strip that is bounded to the north by the Santa Ynez coastal mountains. Average annual rainfall in Santa Barbara is  $\sim 45$  cm and about 95% falls between November and March (Fig. 2). The Santa Barbara watershed is drained by several streams that are mostly intermittent along their lower reaches, including Mission Creek, which flows through the town's center and discharges into the Pacific Ocean within the study site (MacFadden et al., 1991).

Nearly all groundwater recharge and surface water flow is derived from precipitation within the region (Martin, 1984). Principal groundwater-bearing deposits of the regional aquifer system include the alluvium (terrace deposits, poorly-sorted sands, gravel, silt and clay) and the Santa Barbara Formation (marine origin, fine to coarse sands, gravel, silt and clays) (Freckleton et al., 1998). Historically, some groundwater has been locally artesian. Under sustained and heavy groundwater pumping along the coast, salt water intrusion is likely to occur wherever the water table of a coastal aquifer approaches sea level. In Santa Barbara, since the early 1960s, the groundwater levels at the coast have been below sea level, and salt water has locally intruded the shallow deposits as water levels have declined. In the late 1970's, groundwater levels declined by more than 30 m in response to increased municipal pumping, and salt water subsequently intruded deeper water-bearing deposits close to the coast. Presently, salt water intrusion along coastal Santa Barbara is carefully monitored (Martin, 1984).

Winter precipitation events can deliver substantial amounts of dissolved and particulate nitrogen, phosphate, and carbon to the coastal ocean, particularly from watersheds heavily influenced by agriculture and urban development (Beighley et al., 2008). During winter months, marine nitrogen inputs tend to be low, which contributes to a strong seasonality in both physical and geochemical signals in the coastal waters off Santa Barbara (Warrick et al., 2005; McFee-Shaw et al., 2007).

### 3. Field and analytical methods

#### 3.1. Groundwater

A set of shallow monitoring wells, located either along a shore-perpendicular beach transect (Fig. 3), or within close proximity of the beach, were sampled in mid-November 2005, late May/early June 2006, and in mid-April 2007 for groundwater  $^{222}\text{Rn}$ ,  $^{223,224,226,228}\text{Ra}$ , nutrients ( $\text{NH}_4^+$ ,  $\text{SiO}_4$ ,  $\text{PO}_4^{3-}$ ,  $[\text{NO}_2^- + \text{NO}_3^-]$ , DIN, TDN, and DON). For the duration of the study, groundwater levels in these monitoring wells were continuously recorded with pressure transducers and manually confirmed using a hydro-tape (Izbicki et al., in review). During each of the three sampling efforts, the monitoring wells were sampled following standard USGS protocols that included purging at least three well volumes before sample collection. In April 2007, a temporary well ('tempwell') was installed just landward of the high tide line by excavating sand to a depth of 1.5 m and installing a 10 cm diameter slotted irrigation pipe that was also screened to exclude larger-sized particulates. This tempwell was instrumented with a Solinst CTD DIVER to monitor salinity, temperature, and water levels (pressure), and also continuously (30 min updates) sampled for  $^{222}\text{Rn}$  using one RAD7  $^{222}\text{Rn}$  monitor. The tempwell was sampled for a suite of nutrients and trace metals, before, during, and after a low tide event. The tempwell groundwater time-series was also complemented with simultaneous water column grab samples collected in the adjacent swash zone ('surface water'), as well as with a suite of time-series samples collected in the adjacent shallow groundwater well SB7 (see Fig. 3 for locations of SB7, tempwell, and surface water sites). Nutrients were immediately preserved in the field and analyzed at the Woods Hole Oceanographic Institution (WHOI) nutrient facility as per methods described in Charette and Buesseler (2004).

#### 3.2. Surface water column

The near-shore coastal waters adjacent to Santa Barbara harbor and beach were sampled to achieve the following three objectives: (1) continuous  $^{222}\text{Rn}$  surveys were first used to identify potential SGD 'hotspots' where elevated  $^{222}\text{Rn}$  might reveal enhanced

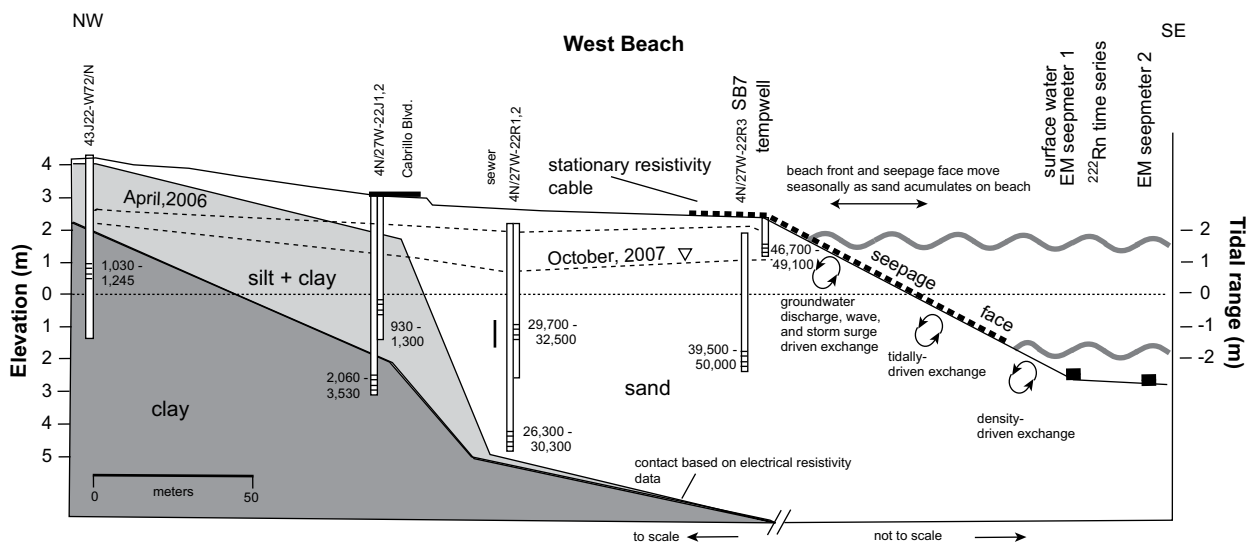


**Fig. 3.** Idealized shore-perpendicular cross-section, showing approximate configuration of clay, silt + clay, and sand layers relative to the land/sea interface. The position of the stationary, shore-perpendicular resistivity line, shown in Fig. 5, is illustrated, as are the relative positions of the two EM seepmeters (Fig. 6) and the 2007 time-series sampling sites for the tempwell, surface water sampling sites, and SB07 (Figs. 7 and 10). Observed groundwater/surface water exchange within this beach front can be expressed as density-, tidal-, or groundwater/wave-driven exchange, or a combination thereof. Ranges in specific conductivity per well reported in  $\text{mS cm}^{-1}$  from 2006 and 2007 sampling data.

advective exchange across the sediment/water interface; (2)  $^{222}\text{Rn}$  time-series measurements just seaward of the low tide line off the beach were used to derive total (fresh + saline) SGD rates from a mass balance model; and (3) ~3 km long offshore transects of  $^{222}\text{Rn}$  and  $^{223,224,226,228}\text{Ra}$  were used to examine offshore constituent gradients, water mass mixing coefficients ( $K_h$ ), apparent Ra ages, and ultimately, a more regional assessment of SGD.

The surface water column was sampled during November 2005, May/June 2006, and April 2007 using a submersible pump that was either attached to a weight placed on the seafloor (near-shore  $^{222}\text{Rn}$  time-series) or suspended 0.5 m from the water surface off a small boat's gunwale ( $^{222}\text{Rn}$  surveys and offshore transects). During the first field campaign (November 2005), multi-day radon surveys were conducted prior to the installation of time-series stations and were used as a guide in their placement relative to shore. For the  $^{222}\text{Rn}$  time-series measurements, a dedicated tender anchored just seaward of the low tide line housed two RAD7  $^{222}\text{Rn}$  detectors plumbed in parallel into a single air–water exchanger (Burnett et al., 2001, 2003, 2006; Dulaiova et al., 2005) that was fed by an instrumented (YSI-multi-probe) bottom water stream via a submersible bilge pump. Air from the exchanger was routed to one or more RAD7 detectors that quantified  $^{222}\text{Rn}$  from the decay of its two alpha-emitting daughter isotopes,  $^{214}\text{Po}$  ( $t_{1/2} = 3.03$  min) and  $^{218}\text{Po}$  ( $t_{1/2} = 1.6 \times 10^{-4}$  s). During each sampling event,  $^{222}\text{Rn}$  was also measured in ambient air using one dedicated RAD7 detector. For Ra isotope analyses, large volumes (20–100 L) of water were passed through individual  $\text{MnO}_2$  impregnated acrylic fiber cartridges (Moore, 2000a; Moore and de Oliveira, 2008). Ra-223,224 activities were quantified from partially dried fibers using delayed coincidence counters (Moore and Arnold, 1996; Moore, 2000b). An ultra-low background HPGe well gamma counter was subsequently used to quantify  $^{226,228}\text{Ra}$  (351.42, 609.31, 338.42, and 911.16 keV, respectively) from the same fiber sample after a chemical elution and  $\text{BaSO}_4$  co-precipitation (Swarzenski et al., 2007c). Reported errors for Ra and Rn are typically <10%. Water column nutrient and trace element samples were collected following clean sampling procedures, including in-line filtration (individual 0.4  $\mu\text{m}$  cartridge filters) and cold storage.

### 3.3. Electrical resistivity

The use of electrical resistivity to examine the fresh water/salt water interface in coastal groundwater is well established (cf. Manheim et al., 2004) and has been enhanced by recent improvements in streamer configuration, as well as data acquisition and processing firmware and software (Swarzenski et al., 2006a,b, 2007a,b). In Santa Barbara, both land-based, stationary resistivity (56 electrodes, spaced 2 m apart) and marine continuous resistivity profiling (two current, nine potential electrodes, spaced 10 m apart) surveys were conducted during each field

campaign. To help define the shallow hydrogeology at the site, only one land-based time-series survey (high and low tide comparison) and one adjacent continuous resistivity profile are presented here.

In stationary mode, an Advanced Geosciences Inc. (AGI) external switching box connected to an R8 SuperSting multi-channel receiver controlled the current flow along the 56-electrode cable (Swarzenski et al., 2006a, 2007b). The 112 m stationary cable was oriented either shore-parallel or shore-perpendicular, and each electrode was pinned to the underlying sediment by a stainless steel 35 cm spike. The relative elevation of each electrode was measured using a laser level and the topography/bathymetry data were then incorporated into inverse modeling routines (AGI EarthImager). In continuous marine mode, the 120 m cable was pulled at a speed of ~3–4 kts on the surface of the water column (Swarzenski et al., 2006b). Real-time GPS data was simultaneously logged into the SuperSting receiver. Polyethylene floats attached to the streamer cable between each electrode were used to keep the cable buoyant on the water surface. Real-time continuous water column salinity/temperature measurements were recorded on an YSI multi-meter, while water depth and the ship's position were recorded on a separate GPS-enabled fathometer system.

### 3.4. Electromagnetic seepage meters

Electromagnetic (EM) seepage meters (Rosenberry and Morin, 2004; Swarzenski et al., 2004) were also deployed continuously for 4–5 days during each field season in the shallow coastal waters off West Beach to physically measure water exchange rates across the sediment/water interface. These meters were pushed into the sandy sediments >15 cm to assure a complete seal around the base of the meter and were generally positioned in a shore-perpendicular configuration such that 1 m (EMS1) was just seaward of the low tide line, and the other meter (EMS2) was positioned slightly further offshore (Fig. 3) in deeper water. The meter display/control panels and power supplies (12 vDC or 120 vAC) were placed on the offshore  $^{222}\text{Rn}$  time-series tender. The EM seepage meters were outfitted with internal- and external-mounted Solinst CTD DIVERS to continuously monitor the salinity, pressure, and temperature both inside and outside the seepage meter domes. Each meter recorded the bi-directional (+ or –) flow rate once every minute.

## 4. Results and discussion

A compilation of the range in specific conductivity, and  $^{223,224,226,228}\text{Ra}$  and  $^{222}\text{Rn}$  activities, from a suite of monitoring well samples (November 2005, May/June 2006, April 2007), the 2007 tempwell samples, and from the adjacent sea water column are listed in Table 1. Groundwater collected from the wells exhibited a broad range (0.8–47.9  $\text{mS cm}^{-1}$ ) in specific conductivities

**Table 1**

Compilation of specific conductivity ( $\text{mS cm}^{-1}$ ) and  $^{222}\text{Rn}$  and  $^{223,224,226,228}\text{Ra}$  activities ( $\text{dpm m}^{-3}$ ) from select monitoring wells, a temporary well (tempwell), and near-shore surface sea water. The reported error for Ra and Rn is <10%. (x) denotes number of samples reported.

	Spec. Cond. ( $\text{mS cm}^{-1}$ )	$^{222}\text{Rn}$ ( $\text{dpm m}^{-3}$ )	$^{226}\text{Ra}$	$^{228}\text{Ra}$	$^{223}\text{Ra}$	$^{224}\text{Ra}$
<i>Groundwater</i>						
Wells*	0.8–47.9	15,000–134,000 (30)	190–650 (9)	400–3640 (9)	170–430 (9)	360–14100 (9)
April 2007 tempwell	46.7–49.1	257,000–570,500 (90)	260–360 (3)	900–1350 (3)	200–310 (3)	420–8200 (3)
<i>Sea water</i>						
November 2005	40.5–43.6	700–8150 (135)	–	–	–	–
May/June 2006	50.0–54.5	580–11,300 (587)	55–120 (8)	23–150 (8)	3–37 (8)	30–530 (8)
April 2007	39.1–51.4	1190–7380 (414)	81–130 (8)	11–210 (8)	17–120 (6)	12–140 (6)

\* All samples (November 2005, May/June 2006, and April 2007).

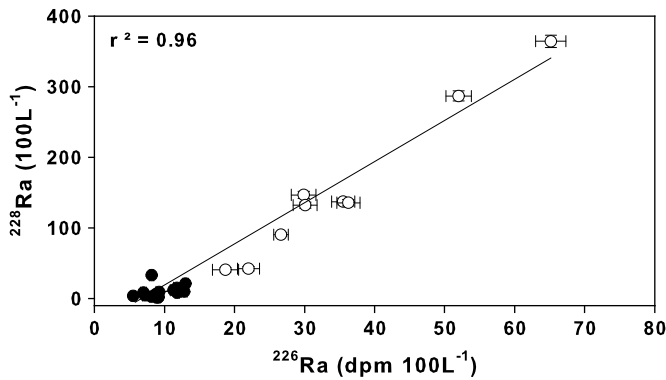


**Fig. 4.** Plot of combined (November 2005, May/June 2006, and April 2007)  $^{226}\text{Ra}$  versus  $^{228}\text{Ra}$  activities ( $\text{dpm } 100\text{L}^{-1}$ ) in coastal surface ( $\bullet$ ) and groundwater ( $\circ$ ) samples at Santa Barbara, California.

depending on distance from the shoreline and screen depths, and approached the upper limit of observed sea water values ( $39.1\text{--}54.4\text{ mS cm}^{-1}$ ). Specific conductivities and water level data from wells along the shore-perpendicular transect (Fig. 3) revealed no significant net discharge of shallow, fresh groundwater to the coastal ocean during the dry season. During winter months, enhanced runoff and precipitation can collect along the upper beach in surface pools that eventually discharge along the beach seepage face as brackish fluxes (Izbicki et al., in review).

Fig. 4 shows a plot of all near-shore surface water and groundwater  $^{228,226}\text{Ra}$  activities. Surface waters were typically elevated in the two Th-series Ra isotopes ( $^{228,224}\text{Ra}$ ) relative to the two U-series Ra isotopes ( $^{226,223}\text{Ra}$ ). There is a strong linear trend in both sets of  $^{226,228}\text{Ra}$  samples, suggesting that Ra is diluted in surface waters from a common groundwater source. The four Ra isotope activities ( $^{223,224,226,228}\text{Ra}$ ) were generally much higher in the surrounding monitoring well samples than in the shallow tempwell samples. This attribute illustrates the hydrogeologic controls on groundwater radionuclide activity, including changes in the subsurface salinity and residence (flushing) times. In contrast,  $^{222}\text{Rn}$  activities were highest in the tempwell (mean =  $463 \pm 61\text{ dpm L}^{-1}$ ) and attained values up to two orders of magnitude greater than near-shore surface waters (mean =  $4\text{ dpm L}^{-1}$ ). Nonetheless, these near-shore surface waters adjacent to West Beach were enriched in the two short-lived  $^{223,224}\text{Ra}$  and  $^{222}\text{Rn}$  relative to more distal sea water.

Groundwater and surface water nutrient ( $\text{NH}_4^+$ ,  $\text{SiO}_4$ ,  $\text{PO}_4^{3-}$ ,  $[\text{NO}_2^- + \text{NO}_3^-]$ , dissolved inorganic nitrogen (DIN =  $[\text{NH}_4^+ + \text{NO}_2^- + \text{NO}_3^-]$ ), dissolved organic nitrogen (DON), and total dissolved nitrogen (TDN)) concentrations per sampling campaign are summarized in Table 2. In general, there is little inter-

**Table 3**

Summary of mean submarine groundwater discharge rates (in  $\text{cm day}^{-1}$ ), as calculated from stationary  $^{222}\text{Rn}$  time-series (ts) deployments in the near-shore surface water column, electromagnetic seepmeters (EMS1 was always positioned closer to the low tide line than EMS2), and from excess  $^{226}\text{Ra}$  and  $^{222}\text{Rn}$  transect (trans.) measurements (see Section 4.3 for discussion).

	$^{222}\text{Rn}$ (ts)	EMS1	EMS2	$^{226}\text{Ra}$ (trans.)	$^{222}\text{Rn}$ (trans.)
	$\text{cm day}^{-1}$				
November 2005	$3.1 \pm 2.6$	$-0.3 \pm 1.0$	$6.0 \pm 4.2$	–	–
May/June 2006	$9.2 \pm 0.8$	$-6.7 \pm 3.1$	$0.9 \pm 5.2$	–	–
April 2007	$6.5 \pm 9.0$	–	$14.5 \pm 55.4$	9.6	7.8

annual variation in groundwater nutrient concentrations, although in April 2007 the shallow beach well (SB07) and the tempwell exhibited distinctly different nutrient concentrations from those found in the monitoring wells. As expected, near-shore surface waters contained much lower nutrient concentrations than the adjacent groundwater, although this trend did not hold for DON, which was slightly greater in the surface water.

Electromagnetic seepmeter results yielded rates that were both positive (net upward flow = submarine groundwater discharge) and negative (net downward flow = sea water infiltration), depending on the meter's location relative to shore, the tidal stage, time of year (frequency and intensity of precipitation), and occurrence of antecedent storms. The observed range ( $-6.7$  to  $14.5\text{ cm day}^{-1}$ ) in advective rates, while low in comparison to other coastal sites (Swarzenski et al., 2007a), did reveal inter-annual variations (Table 3).

#### 4.1. Electrical resistivity

Only two examples of electrical resistivity surveys are presented here; one (Fig. 5A,B) consists of a land-based time-series (low tide/high tide) comparison across the beach face (see Figs. 1 and 3 for approximate orientation of the land-based streamer), while the other (Fig. 5C) is an adjacent marine continuous resistivity profile (CRP). The CRP data was collected by placing the streamer end at the shoreline and then running a shore-perpendicular 853 m transect offshore (see Fig. 1 for CRP transect location). Resistivity values are reported in Ohm-m.

Multi-electrode resistivity provides a useful means of examining the subsurface salinity structure to depths  $>20\text{ m}$ . Because the position of the land-based streamer is fixed during the high tide/low tide time-series and the data collection/inversion parameters remain constant, the observed change in resistivity must be due only to tidally modulated pore-fluid exchange. From Fig. 5A, the highest resistivity values (i.e., freshest groundwater) appear focused under the high tide water line, at a depth of about

**Table 2**

Mean groundwater and near-shore surface water nutrient concentrations ( $\mu\text{M}$ ). Location of groundwater well sites described in Izbicki et al. (in review). Relative position of the surface water, tempwell, and SB07 time-series\* samples relative to the beach face provided in Fig. 3.

	$\text{NH}_4^+$	$\text{SiO}_4$	$\text{PO}_4^{3-}$	$[\text{NO}_2^- + \text{NO}_3^-]$	DIN	DON	TDN	n
	$(\mu\text{M})$							
<i>Groundwater</i>								
November 2005	$64.7 \pm 8.4$	$145.6 \pm 15.6$	$36 \pm 2.4$	$0.1 \pm 0.2$	$64.8 \pm 8.5$	–	–	9
May/June 2006	$62.1 \pm 2.8$	$200.5 \pm 5.1$	$37.5 \pm 3.6$	$0.1 \pm 0$	$62.1 \pm 2.8$	$20.5 \pm 2.1$	$82.6 \pm 4.1$	11
April 2007 tempwell*	$17.4 \pm 2.4$	$122.7 \pm 35.5$	$11.6 \pm 3.3$	$158.6 \pm 42.9$	$176 \pm 41.3$	$24.2 \pm 24.9$	$200.2 \pm 61.4$	14
April 2007 SB07*	$39.5 \pm 2.4$	$272.2 \pm 31.8$	$54.9 \pm 6.8$	$0.1 \pm 0$	$39.5 \pm 2.5$	$28.2 \pm 4.1$	$67.7 \pm 3.6$	14
Mean	$45.9 \pm 4$	$185.2 \pm 22$	$35 \pm 4$	$39.7 \pm 10.8$	$85.6 \pm 13.8$	$24.3 \pm 10.3$	$116.8 \pm 23$	
<i>Sea water</i>								
November 2005	$8.7 \pm 7.7$	$15 \pm 4.1$	$2.2 \pm 1.5$	$0.3 \pm 0.2$	$9 \pm 7.7$	–	–	9
April 2007*	$13 \pm 13.7$	$30.3 \pm 9.2$	$3.2 \pm 2.8$	$17.4 \pm 7.8$	$30.4 \pm 14.1$	$33.3 \pm 60.5$	$63.7 \pm 69.1$	14
Mean	$10.9 \pm 10.7$	$22.6 \pm 6.6$	$2.7 \pm 2.2$	$8.9 \pm 4$	$19.7 \pm 10.9$	–	–	

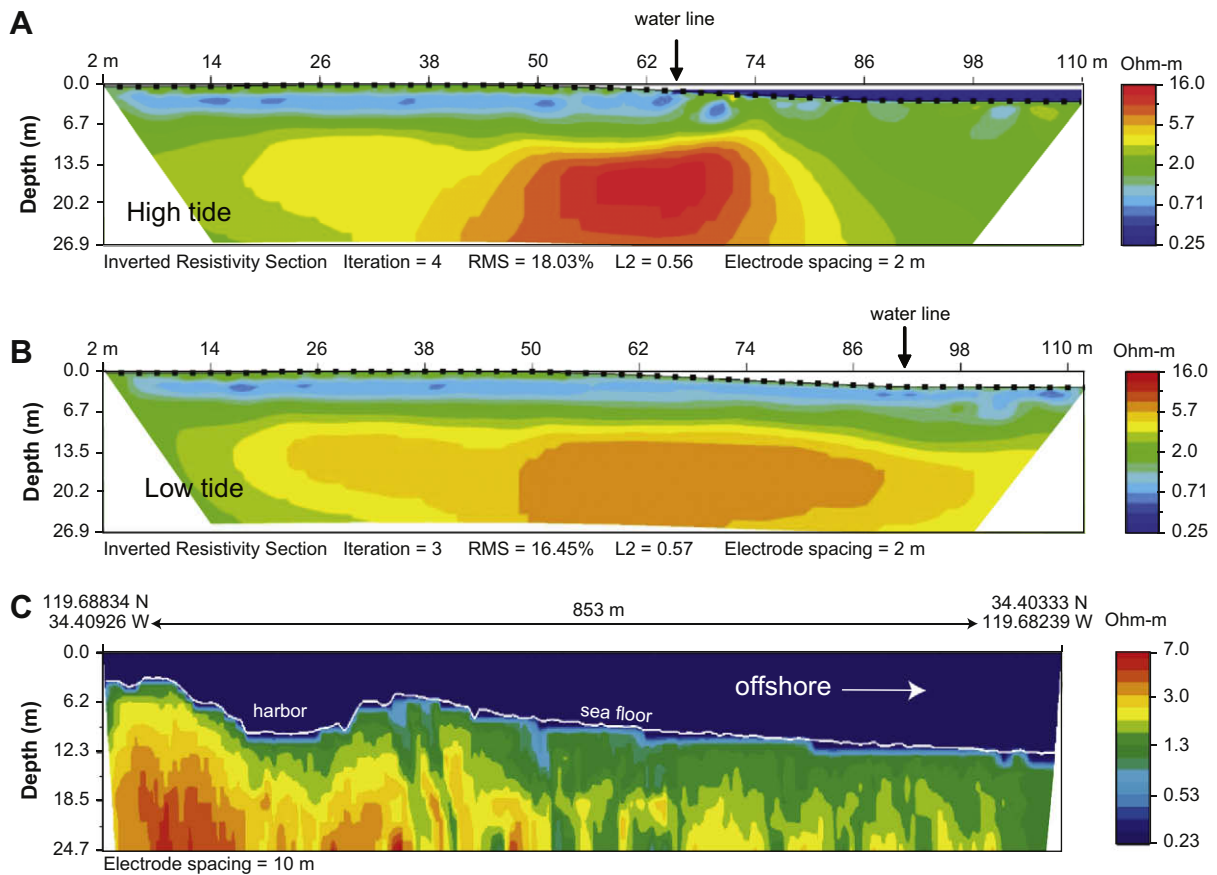


**Fig. 5.** Inverted resistivity image of the beach face during high (A); and low (B) tide. The tidal range was  $\sim 2$  m. Approximate position of the shore-perpendicular oriented land-based streamer cable relative to the beach face is shown in Fig. 3. (C) Shows a marine continuous resistivity profile (CRP) survey of an 853 m line adjacent to the A-A' primary transect. Location of this transect line is illustrated in Fig. 1.

15 m. In contrast, at low tide (Fig. 5B), the zone of higher resistivity is stretched much further offshore, past the low tide water line ( $\sim 50$  m). The resistivity images show a shallow saline water wedge positioned on top of the water table and provide further evidence that there is likely no significant discharge of freshened groundwater along the beach face within the depths studied. Instead, it appears that the saline pore fluids respond more to tidal forcing; during high tide, incoming sea water pushes against the groundwater lens which consequently gets backed up close to the high tide line. At low tide, this pressure is released by a falling water table and the groundwater lens can migrate further seaward, inducing mixing within a zone of enhanced SGD that extends 50 m or so from shore. This tidally driven exchange likely discharges some SGD into the water column during every low tide event that is captured by the  $^{222}\text{Rn}$  time-series and the EM seepmeters.

Marine continuous resistivity profiling (CRP) surveys were conducted in November 2005 and May/June 2006 in concert with the Rn surveys, and allow large datasets of subsurface resistivity to be collected (boat speed  $\sim 3\text{--}4$  kts). However, without additional groundtruthing measures (i.e., core logs, pore water salinities, sediment resistivities), it is often difficult to extract more than qualitative information from such data. The modeled resistivity image shown in Fig. 9C shows an expected 'freshening' closest to shore at a depth  $>15$  m. The CRP resistivity range is comparable to values derived from the land-based surveys (Fig. 5A,B), and confirms that no obvious discharge of reduced-salinity groundwater occurs beyond  $\sim 50$  m from shore.

#### 4.2. Time-series

To develop a mass balance model for submarine groundwater discharge, a time-series of excess  $^{222}\text{Rn}$  in near-shore surface water was utilized (Burnett and Dulaiova, 2003; Burnett et al., 2003, 2006, 2007, 2008; Dulaiova et al., 2005, 2006a,b; Swarzenski et al., 2006b, 2007a; Weinstein et al., 2007). The premise of this technique relies on converting near-continuous excess  $^{222}\text{Rn}$  (accounting for a mean parent  $^{226}\text{Ra}$  water column activity) measurements ( $\text{dpm m}^{-3}$ ) into inventories ( $\text{dpm m}^{-2}$ ) using real-time water-level data. Rn-222 inventories are subsequently converted into hourly fluxes ( $\text{dpm m}^{-2} \text{h}^{-1}$ ) and then corrected for both tidal radon exchanges (positive as offshore  $^{222}\text{Rn}$  brought in by an inflowing tide and negative as  $^{222}\text{Rn}$  lost during an outflowing tide) and atmospheric  $^{222}\text{Rn}$  losses.

Fig. 6D shows a representative example of a multi-day  $^{222}\text{Rn}$  time-series in November 2005, as a function of (Fig. 6A) tidal water level variations and specific conductivity. During this time-series, each low tide event was marked with a pulse of heightened SGD, as recorded also by the EM seepage meters (Fig. 6B,C) as well as the specific conductivity record that revealed that the salinity of the shallow groundwater was actually higher than the near-shore waters. Interestingly, EM seepage meter 1 showed distinct low tide-coincident pulses in spite of mostly net negative SGD rates and that slightly more saline water escaped the sediment/water interface at low tide relative to the surface water salinities. While the overall pattern of SGD, as quantified by the two EM seepage meters, shows some similar features, the mean rates (EM seepage meter 1 =  $-0.3 \pm 1.0 \text{ cm day}^{-1}$ ; EM seepage meter 2 =  $6.0 \pm 4.2 \text{ cm day}^{-1}$ ) reflect the different placement of the two seepmeters

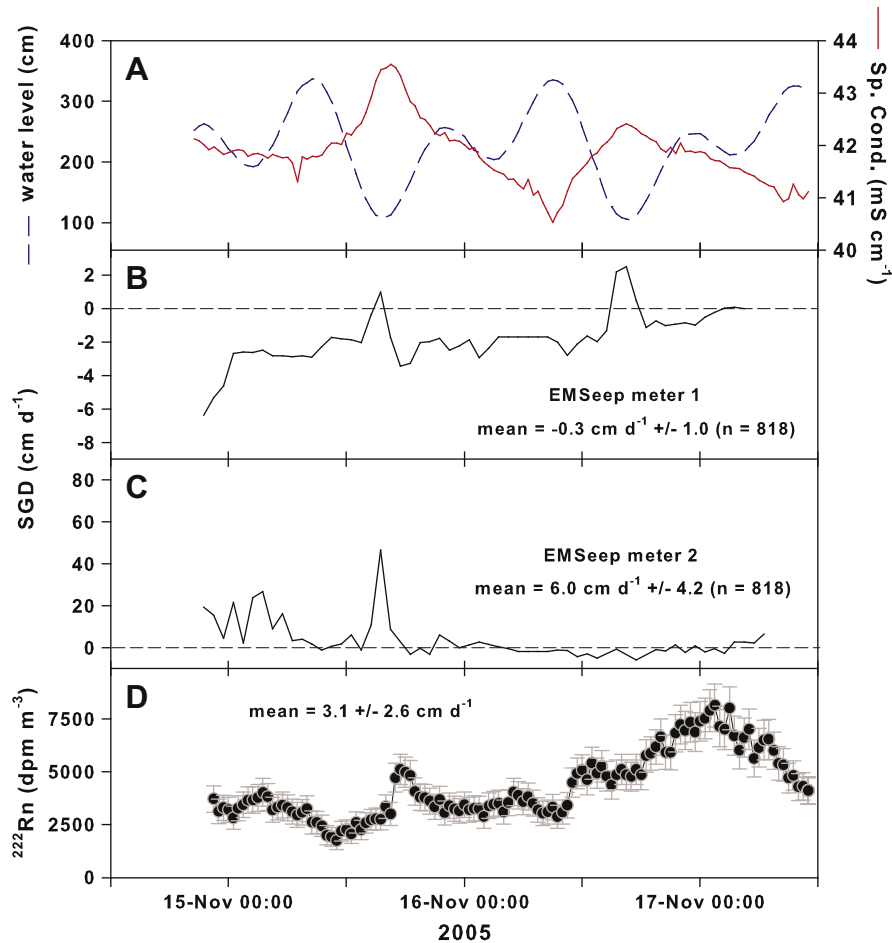


**Fig. 6.** Water column time-series (November, 2005), showing: (A) water level (tide), specific conductivity ( $\text{mS cm}^{-1}$ ); (B, C) advective SGD rates derived from electromagnetic (EM) seepmeters ( $\text{cm day}^{-1}$ ); and (D)  $^{222}\text{Rn}$  activities ( $\text{dpm m}^{-3}$ ). Note low tide coincident pulses in specific conductivities, EM seepmeter derived advective rates, and  $^{222}\text{Rn}$ .

relative to the shoreline, and thus water depth. EMS1 was positioned further inshore, just seaward of the low tide line, than EMS2. From both EM seepage meter records, one can infer subtle nuances in SGD. For example, it is likely that EMS1 responded more to tidally-modulated shallow exchange processes that occurred within the beach face as shallow saline circulation cells (Robinson et al., 2007b) (see Fig. 3). Such discharge could have both physical and hydrologic controls. The passage of a high-energy storm just prior to sampling could push sea water much further up the beach face where recharge, subsurface flow, and eventual offshore discharge would influence the salinity and flow rates of SGD.

To be able to convert near-shore total  $^{222}\text{Rn}$  fluxes ( $\text{dpm m}^{-2} \text{h}^{-1}$ ) into advective exchange rates ( $\text{cm}^3 \text{cm}^{-2} \text{day}^{-1}$ ), a representative groundwater endmember activity must be quantified. A groundwater  $^{222}\text{Rn}$  time-series was collected within the high tide line tempwell, which was also monitored for continuous water levels and specific conductivities (Fig. 7). Fig. 7A shows tidally-driven, water level variations of near-shore surface waters, while a record of tempwell water levels and specific conductivities is shown in Fig. 7B. A slight increase in the salinity in the tempwell appears coincident with the first low tide event, but sustained pumping ran the tempwell temporarily dry, and the interruption in the water flow was recorded as a break in  $^{222}\text{Rn}$  and specific conductivity values. Accounting for this interruption, the groundwater  $^{222}\text{Rn}$  within the tempwell ranged (Fig. 7C) from  $\sim 360$  to  $570 \text{ dpm L}^{-1}$ , with a mean of  $463 \pm 61 \text{ dpm L}^{-1}$  ( $n = 90$ ). This value is considerably higher than the range in  $^{222}\text{Rn}$  observed (15–

$134 \text{ dpm L}^{-1}$ ) within the suite of groundwater monitoring wells adjacent to West Beach and does reflect more closely the water that is actually involved in the near-shore exchange. Dividing the total  $^{222}\text{Rn}$  fluxes by this groundwater  $^{222}\text{Rn}$  value results in a mean SGD rate of  $3.1 \pm 2.6 \text{ cm day}^{-1}$ . Such SGD rates were also calculated for the 2006 and 2007  $^{222}\text{Rn}$  time-series deployments and are reported in Table 3. If we estimate from land-based resistivity data a narrow seepage face of  $\sim 50 \text{ m}$ , then these advective rates would correspond to  $1.5\text{--}4.6 \text{ m}^3$  of groundwater exchanged per day, per meter of shoreline. These results compare favorably to similar values obtained from the EM seepmeters, which yield a flux of  $0.5\text{--}7.3 \text{ m}^3 \text{m}^{-1} \text{day}^{-1}$ .

#### 4.3. Offshore Ra and Rn transects

In coastal waters where water mass mixing is more a function of eddy diffusion than advection processes, it has been shown (Moore, 2000a) that the two short-lived Ra isotopes ( $^{223}\text{Ra} = 11.3 \text{ day}$ ;  $^{224}\text{Ra} = 3.66 \text{ day}$ ) can be used effectively to obtain Ra-derived apparent water mass ages (Fig. 8A) and eddy diffusion coefficients,  $K_h$  ( $\text{m}^2 \text{s}^{-1}$ ). The premise of this method is that all Ra inputs occur only at the shoreline (i.e., surface water column is stratified) and Ra losses occur only as a function of radioactive decay. Water mass mixing rates can then be derived from the slope of a natural logarithm of either Ra isotope as a function of distance from shore. During the April 2007 sampling, the near-shore surface water column was stratified due to thermal heating (<http://www.lternet>.

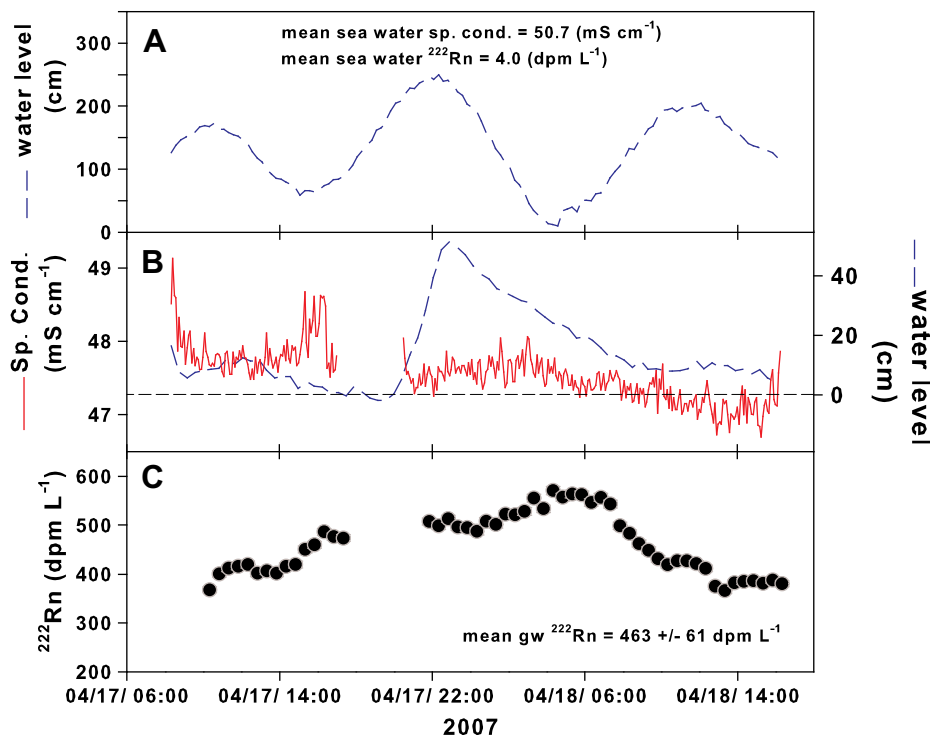


**Fig. 7.** Groundwater  $^{222}\text{Rn}$  time-series (C) from a temporary 1.5 m deep well (“tempwell”), positioned just landward of the high tide line (see Fig. 3 for relative location). The tempwell water level decline (B) is reflected in both Rn and specific conductivity ( $\text{mS cm}^{-1}$ ). A mean groundwater  $^{222}\text{Rn}$  activity ( $\bullet$ ) of  $463 \pm 61 \text{ dpm L}^{-1}$  is used for water column time-series and offshore transect  $^{222}\text{Rn}$ -derived SGD derivations. Note mean near-shore surface water  $^{222}\text{Rn}$  activity of  $4.0 \text{ dpm L}^{-1}$  and near-shore tidal fluctuation (A).

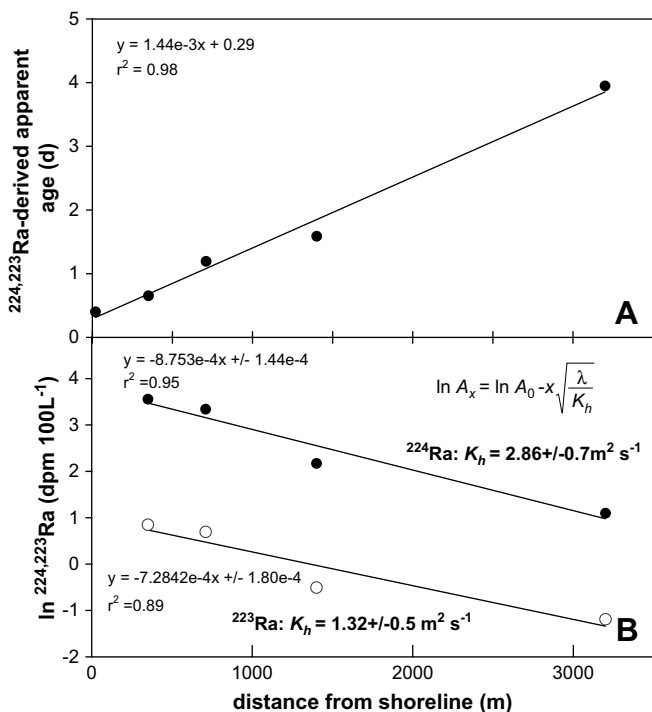


**Fig. 8.** (A) Plot of  $^{223,224}\text{Ra}$ -derived apparent water mass ages (“Ra-ages”) as a function of distance offshore (m); and (B)  $\ln^{223,224}\text{Ra}$  activity as a function of distance from shore used to derive eddy diffusion coefficients,  $K_h$ . The offshore transect was conducted in June 2006. At 3200 m (the distal station), the water depth was 34.2 m and the surface water column was stratified due to thermal heating and wind mixing (<http://sbc.lternet.edu/data>).

[edu/sites/sbc/](http://sbc.lternet.edu/sites/sbc/)). Fig. 8B shows a plot of  $\ln^{223,224}\text{Ra}$  versus distance from the West Beach shoreline collected during the April 2007 field season. The  $\ln^{223}\text{Ra}$  regression had a slope of  $-7.28e-1 \pm 1.80e-1 \text{ km}^{-1}$  from which a mixing coefficient  $K_h$  of  $1.32 \pm 0.5 \text{ m}^2 \text{ s}^{-1}$  was calculated using Eq. (1):

$$\text{slope} = \sqrt{\frac{\lambda}{K_h}} \quad (1)$$

A  $K_h$  of  $2.86 \pm 0.7 \text{ m}^2 \text{ s}^{-1}$  can be similarly calculated from  $\ln^{224}\text{Ra}$ . Differences in these two  $K_h$  values reflect the difference in the half-lives of  $^{223,224}\text{Ra}$ . Nonetheless, these  $K_h$  values are comparable to other such estimates, as calculated for example off close-by Huntington Beach, California (Boehm et al., 2004; Colbert and Hammond, 2007a,b).

Once these eddy diffusion coefficients have been calculated, one can re-examine the offshore  $^{226}\text{Ra}$  distribution to derive another measure of SGD (e.g., Moore and de Oliveira, 2008; Burnett et al., 2008). The flux of  $^{226}\text{Ra}$  away from our study site at West Beach can be expressed as a product of  $^{223}\text{Ra}$ -derived  $K_h$  multiplied by the offshore  $^{226}\text{Ra}$  gradient and the thickness of the mixed layer. A linear  $^{226}\text{Ra}$  gradient of  $-13.79 \pm 5.6 \text{ dpm m}^{-3}$  per km was calculated along a 3.2 km transect using a mean near-shore surface water  $^{226}\text{Ra}$  activity of  $125.48 \pm 6.5 \text{ dpm m}^{-3}$  ( $n = 3$ ) and an offshore value of  $82 \pm 0.5 \text{ dpm m}^{-3}$  ( $n = 3$ ). In the absence of rivers or streams that could introduce ‘new’ Ra into the coastal waters, the calculated offshore  $^{226}\text{Ra}$  flux of  $1.6 \pm 0.8 \times 10^6 \text{ dpm km}^{-1} \text{ day}^{-1}$  using the  $^{223}\text{Ra}$ -derived  $K_h$  and a water parcel depth of 1 m must be balanced by an equal groundwater exchange term. Three groundwater  $^{226}\text{Ra}$  values (mean  $^{226}\text{Ra} = 328.1 \pm 53.5 \text{ dpm m}^{-3}$ ) were obtained from the tempwell. Dividing the offshore  $^{226}\text{Ra}$  flux by this groundwater term yields a groundwater exchange rate of  $4.8 \pm 3 \text{ m}^3 \text{ m}^{-1} \text{ day}^{-1}$ , which corresponds to  $9.6 \text{ cm day}^{-1}$ , if we

assume again that Ra enters the water column within a 50 m wide band, as defined earlier by land-based resistivity. This SGD rate is very close to the similarly calculated SGD rate ( $\sim 6\text{--}13\text{ m}^3\text{ m}^{-1}\text{ day}^{-1}$ ) obtained at Huntington Beach, California by Boehm et al. (2006).

During the offshore transect Ra sampling, the surface waters were also continuously analyzed for  $^{222}\text{Rn}$  using four RAD7s. As each Ra sampling event lasted over 1 h, the RAD7s simultaneously recorded the  $^{222}\text{Rn}$  concentration at each Ra station. The distribution of  $^{222}\text{Rn}$  along the same shore-perpendicular transect can be similarly examined to obtain further SGD and mixing rate information, including combined atmospheric loss and radioactive decay terms. Based on an average Rn value obtained from multiple readings observed at each offshore station, a linear  $^{222}\text{Rn}$  activity gradient of  $-1.17\text{ dpm m}^{-3}$  per m was obtained using the April 2007 near-shore  $^{222}\text{Rn}$  time-series data (mean =  $4040 \pm 1171\text{ dpm m}^{-3}$ ) and a mean offshore  $^{222}\text{Rn}$  activity of  $330\text{ dpm m}^{-3}$ . Atmospheric loss terms were negligible relative to the radon inventories. Multiplying this linear  $^{222}\text{Rn}$  gradient by the  $^{223}\text{Ra}$ -derived  $K_h$  yields a total offshore flux of  $1.80 \times 10^6\text{ dpm m}^{-1}\text{ day}^{-1}$ , or  $1503\text{ dpm m}^{-2}\text{ h}^{-1}$  if one integrates this flux across the 50 m wide SGD zone. This  $^{222}\text{Rn}$  flux rate compares well to the mean mixing loss term ( $1290\text{ dpm m}^{-2}\text{ h}^{-1}$ ) calculated from the corresponding surface water column  $^{222}\text{Rn}$  time-series data. Dividing this flux rate by the mean groundwater  $^{222}\text{Rn}$  activity observed in the tempwell (Fig. 7:  $463,000\text{ dpm m}^{-3}$ ) results in a groundwater exchange rate of  $3.9\text{ m}^3\text{ m}^{-1}\text{ day}^{-1}$  (i.e.,  $7.8\text{ cm day}^{-1}$ ) – a value very similar to the rate obtained using  $^{226}\text{Ra}$ . The similarity of these two independent SGD estimates across a single shore-perpendicular transect confirms the utility of these two tracers of SGD, and that in these coastal waters off Santa Barbara, SGD consists of mostly of recycled sea water without a significant fresh water component.

As the half-lives of  $^{224}\text{Ra}$  (3.66 day) and  $^{222}\text{Rn}$  (3.8 day) are so similar, and their respective production rates in sediment are constant and quantifiable, one can use their unique geochemical characteristics in coastal waters to define differential mixing loss terms (Dulaiova and Burnett, 2006). While both  $^{224}\text{Ra}$  and  $^{222}\text{Rn}$  are conveyed into coastal waters by SGD (Ra may have a small additional seasonal riverine source), their estuarine fate is tied directly to water mass mixing and radioactive decay. Additionally,  $^{222}\text{Rn}$ , as a noble gas, can escape the air/sea interface. Because of its strong concentration gradient across this interface in coastal waters, this isotope has been used frequently to study air–water gas exchange. Atmospheric evasion of  $^{222}\text{Rn}$  is usually modeled as a function of molecular diffusion, taking into account Ostwald's solubility coefficient ( $\alpha$ ) and an estimate of the gas transfer velocity,  $k$ , which has been shown to vary complexly as a function of wind speed, temperature, water currents, and water depth (Macintyre et al., 1995). Dulaiova and Burnett (2006) elegantly developed an approach that quantifies the atmospheric  $^{222}\text{Rn}$  loss term independently from a combined  $^{222}\text{Rn}/^{224}\text{Ra}$  isotope method. The premise of this approach is that the  $^{222}\text{Rn}/^{224}\text{Ra}$  ratio should change only as a function of gas evasion terms, including wind speed, currents, water depth, and temperature.

Observed  $^{224}\text{Ra}/^{223}\text{Ra}$  activity ratios along a shore-perpendicular surface water transect and in representative groundwater can be used to estimate apparent ('Ra') water mass ages (Moore 2000). Fig. 8A shows a plot of these 'Ra ages' as a function of distance traveled away from shore. Following the Dulaiova and Burnett's (2006) approach, we decay-normalized the  $^{224}\text{Ra}$  data to the slightly longer-lived  $^{222}\text{Rn}$  and then plotted both isotopes against the  $^{224}\text{Ra}/^{223}\text{Ra}$ -derived apparent ages (Fig. 9). As expected, the  $^{222}\text{Rn}$  slope is much steeper than the  $^{224}\text{Ra}$  slope, indicating preferential radon losses across the air/water interface. To quantify this loss, the  $^{224}\text{Ra}$  line equation is multiplied by a ratio of the two y-intercepts

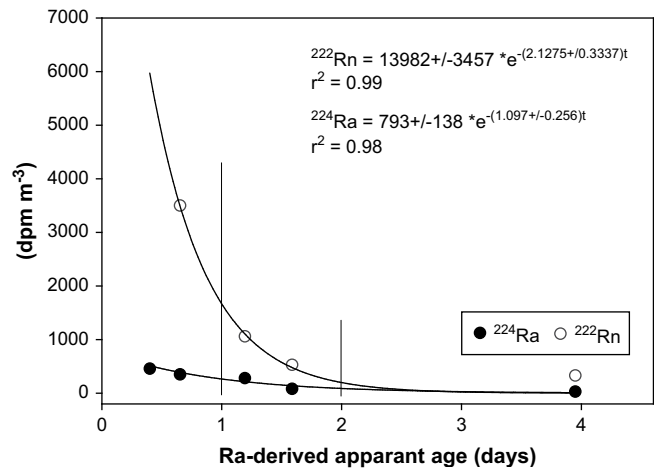


Fig. 9. A plot of decay-normalized  $^{222}\text{Rn}$  ( $\circ$ ) and  $^{224}\text{Ra}$  ( $\bullet$ ) ( $\text{dpm m}^{-3}$ ) as a function of apparent radium ages along an offshore transect (June, 2006) used to estimate the preferential rate of  $^{222}\text{Rn}$  loss from the water column over time ( $\text{dpm m}^{-3}\text{ day}^{-1}$ ) due to atmospheric evasion. Since the two nuclides have similar sources and half-lives, the radon air–water exchange rate can be estimated from the difference in the slopes of the  $^{222}\text{Rn}$  and  $^{224}\text{Ra}$  horizontal distributions.

(13,982/793) and the slope of each line thus represents a total loss rate per time ( $\text{dpm m}^{-3}\text{ day}^{-1}$ ) along the transect. The difference in the  $^{224}\text{Ra}$  and  $^{222}\text{Rn}$  slopes yields an estimate of the  $^{222}\text{Rn}$  evasion rate, which ranged up to  $1400\text{ dpm m}^{-3}\text{ day}^{-1}$  closest to shore, and compared well theoretical model (Macintyre et al., 1995) results.

#### 4.4. SGD-derived nutrient loading

While the geochemical tracers and the electrical resistivity images provide insight into the scales and patterns of total SGD off West Beach, the lack of a significant fresh water component in this SGD signal does not necessarily rule out the possibility that SGD-derived nutrient loadings to these coastal waters must be insignificant. Table 2 provides a summary of the mean nutrient concentrations in a suite of groundwater samples and adjacent surface water from our study site. The tempwell, which was located close to the high tide line (see Fig. 3 for time-series sampling locations along the beach face), had vastly different nutrient concentrations than the suite of surrounding monitoring wells, including nearby SB07 (Fig. 1). For example, mean  $\text{PO}_4^{3-}$ ,  $\text{SiO}_4$  and  $\text{NH}_4^+$  concentrations from the tempwell time-series were all considerably lower than what was observed in the monitoring wells. In contrast, mean  $[\text{NO}_2^- + \text{NO}_3^-]$  concentrations approached  $0\text{ }\mu\text{m}$  in the monitoring well samples (i.e., strongly reducing nature of the regional aquifer deposits), while in the tempwell  $[\text{NO}_2^- + \text{NO}_3^-]$  exceeded a mean value of  $150\text{ }\mu\text{m}$ . Time-series nutrient data (Fig. 10) show tidally modulated  $\text{NH}_4^+$ ,  $\text{PO}_4^{3-}$  and  $\text{SiO}_4$  pulses in the surface waters that appear coincident with a low tide event. The absence of a corresponding  $[\text{NO}_2^- + \text{NO}_3^-]$  peak suggests saline groundwater discharge. Thus, such nutrient profiles provide information as to redox state and residence times of these coastal groundwaters, as well as possible source terms. The position of the tempwell close to the high tide line suggests that  $[\text{NO}_2^- + \text{NO}_3^-]$  inputs may also be locally derived. For example, just above the high tide line a heavy kelp line was actively scavenged by shoreline birds.

Table 2 also summarizes the adjacent sea water nutrient concentrations per season; all are substantially lower than mean near-shore groundwater nutrient concentrations. Such a scenario

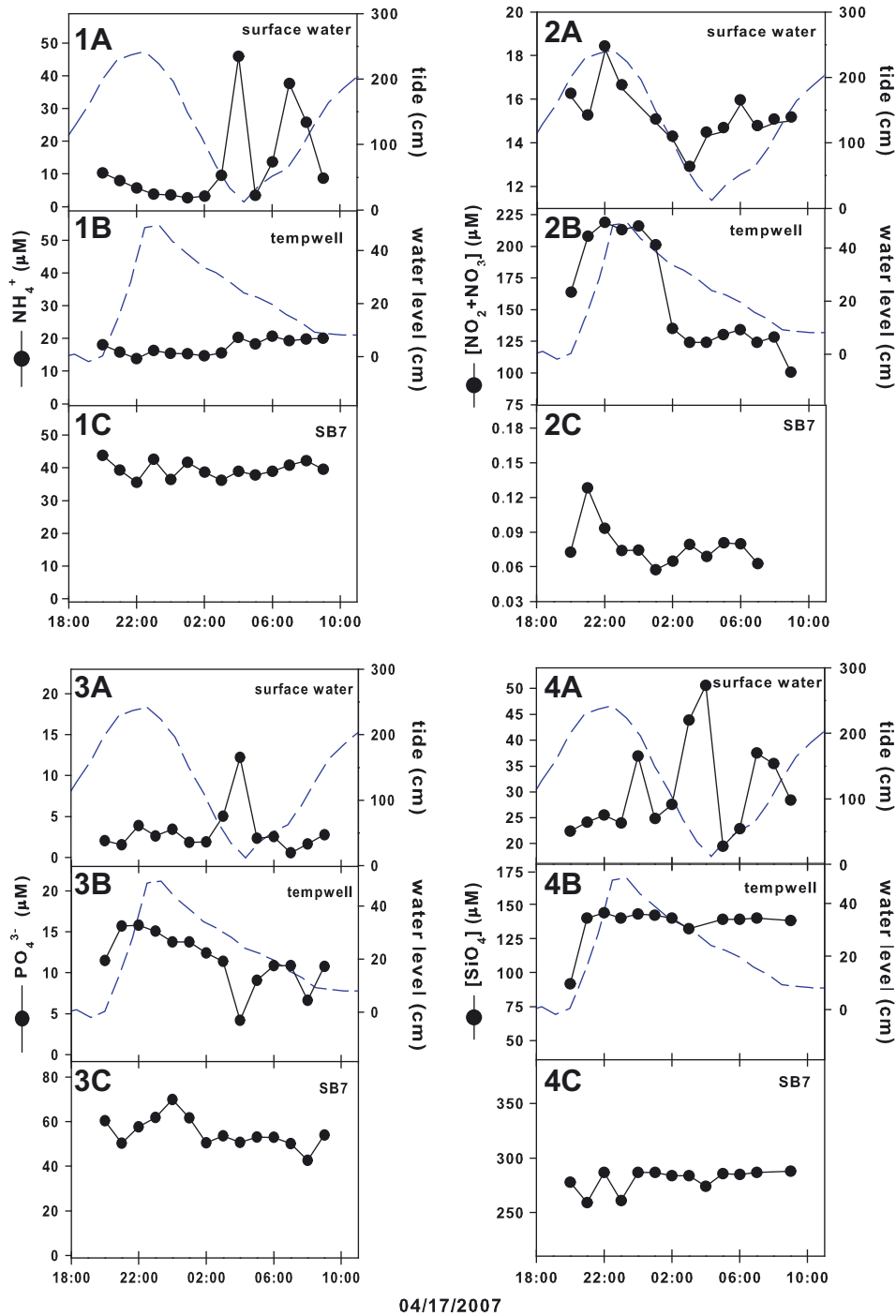


**Fig. 10.** Time-series of dissolved nutrient concentrations ( $\mu\text{M}$ ) (1A–C:  $\text{NH}_4^+$ , 2A–C:  $[\text{NO}_2^- + \text{NO}_3^-]$ , 3A–C:  $\text{PO}_4^{3-}$ , and 4A–C:  $\text{SiO}_4$ ) collected concurrently in near-shore surface water, tempwell, and well SB7 as a function of water level (dashed line). Note scales held constant wherever feasible. Location of tempwell and SB7 relative to high tide line shown in Fig. 3.

sets up a positive concentration gradient that can drive nutrients into near-shore coastal waters with SGD. A summary of calculated SGD rates ( $\text{cm day}^{-1}$ ) is shown in Table 3. Acknowledging conservative nutrient behavior during beach-face transport, one can multiply above SGD rates by the mean groundwater nutrient concentrations to yield the following SGD-derived nutrient loading estimates:  $0.06\text{--}0.29 \text{ mol day}^{-1} \text{ m}^{-1}$  ( $\text{NH}_4^+$ ),  $0.22\text{--}0.92 \text{ mol day}^{-1} \text{ m}^{-1}$  ( $\text{SiO}_4$ ),  $0.04\text{--}0.17 \text{ mol day}^{-1} \text{ m}^{-1}$  ( $\text{PO}_4^{3-}$ ),  $0.10\text{--}0.57 \text{ mol day}^{-1} \text{ m}^{-1}$  (DIN), and  $0.08\text{--}0.09 \text{ mol day}^{-1} \text{ m}^{-1}$  (DON). Such loadings (Table 4) are expectedly lower than similarly computed

estimates for sub-tropical Tampa Bay, Florida (Swarzenski et al., 2007c) or temperate Hood Canal, Washington (Swarzenski et al., 2007a), but similar in magnitude to SGD-derived DIN ( $0.12 \text{ moles day}^{-1} \text{ m}^{-1}$ ) and SRP ( $0.005 \text{ moles day}^{-1} \text{ m}^{-1}$ ) loadings calculated for the coastal waters off Huntington Beach (Boehm et al., 2006). Such results also suggest that a sustained flux of SGD-derived nutrients can be delivered to the near-shore coastal waters off Santa Barbara, California, where riverine nutrient loads are highly seasonal (Warrick et al., 2005; Beighley et al., 2008) and generally much less than the marine-derived nutrient contributions

**Table 4**  
Combined SGD-derived nutrient loading estimates (mol day<sup>-1</sup> per meter of shoreline) for the near-shore coastal waters off Santa Barbara. Cumulative uncertainty includes range in SGD rates and seasonality.

	NH <sub>4</sub> <sup>+</sup> (mol day <sup>-1</sup> m <sup>-1</sup> )	SiO <sub>4</sub>	PO <sub>4</sub> <sup>3-</sup>	[NO <sub>2</sub> + NO <sub>3</sub> ]	DIN	DON	TDN
Range	0.06–0.29	0.22–0.92	0.04–0.17	0–0.52	0.10–0.57	0.08–0.09	0.38–0.65
Mean	0.15	0.51	0.09	0.17	0.32	0.09	0.52
±	0.10	0.30	0.06	0.24	0.01	0.08	0.14

(McFee-Shaw et al., 2007), but where there is no large fresh water SGD component.

#### 4.5. Summary

Repeat geochemical and geophysical measurements have been made on a marine beach and the coastal waters of Santa Barbara, California, to study coastal exchange processes across the land/sea margin, including submarine groundwater discharge (SGD) and associated nutrient loading estimates. The following findings have resulted from this research:

- 1) the geochemical tracers <sup>222</sup>Rn and <sup>223,224,226,228</sup>Ra are present at much greater activities in the shallow groundwater of our study site than in adjacent near-shore sea water. This attribute allows us to use these radionuclides as quantitative tracers of coastal groundwater discharge. Calculated SGD rates ranged from 3.1 ± 2.6 to 9.2 ± 0.8 cm day<sup>-1</sup>, depending on which tracer approach was used and on the sampling season. There was very little difference between Ra- and Rn-derived SGD rates, suggesting that the saline component of SGD obtained from Ra accounts for most of total SGD signal;
- 2) within the constraints of a first-order model, the exponential distribution of <sup>223,224</sup>Ra and <sup>222</sup>Rn in surface waters along a shore-perpendicular transect from the marine beach to >3 km offshore (water depth = 34.2 m) was used to estimate an eddy diffusivity coefficient, *K<sub>h</sub>* (<sup>223</sup>Ra: *K<sub>h</sub>* = 1.32 ± 0.5 m<sup>3</sup> sec<sup>-1</sup>; <sup>224</sup>Ra: *K<sub>h</sub>* = 2.86 ± 0.7 m<sup>3</sup> s<sup>-1</sup>). Since <sup>224</sup>Ra and <sup>222</sup>Rn have similar sources and half-lives, the radon air–water exchange rate can also be estimated from the difference in the slopes of the <sup>222</sup>Rn and <sup>224</sup>Ra horizontal distributions. Combined <sup>222</sup>Rn/<sup>224</sup>Ra water column removal terms yield observed air/sea evasion rates that are very similar to theoretical model (Macintyre et al., 1995) results;
- 3) electromagnetic seepage meter deployments in the near-shore waters recorded both discharge (positive) and recharge (negative) events that are tidally modulated, and ranged from -0.3 ± 1.0 to 14.5 ± 55.4 cm day<sup>-1</sup>, depending on the position of the meter relative to shoreline and the sampling season. Low tide coincident pulses in EM seepmeter data also showed a spike in salinity. Such discharge is likely also driven by past sea water intrusion events during storms and subsequent seepage of saline groundwater;
- 4) nutrients (NH<sub>4</sub><sup>+</sup>, SiO<sub>4</sub>, PO<sub>4</sub><sup>3-</sup>, [NO<sub>2</sub> + NO<sub>3</sub>], DIN, TDN, and DON) were also quantified in shallow groundwater and the near-shore coastal waters and used to calculate SGD-derived nutrient loading estimates. Depending on the sampling season and on the particular the SGD tracer used, the following nutrient loads were calculated: NH<sub>4</sub><sup>+</sup> = 0.06–0.29 mol day<sup>-1</sup> m<sup>-1</sup>; SiO<sub>4</sub> = 0.22–0.29 mol day<sup>-1</sup> m<sup>-1</sup>; PO<sub>4</sub><sup>3-</sup> = 0.04–0.17 mol day<sup>-1</sup> m<sup>-1</sup>; [NO<sub>2</sub> + NO<sub>3</sub>] = 0–0.52 mol day<sup>-1</sup> m<sup>-1</sup>; dissolved inorganic nitrogen (DIN) = 0.01–0.17 mol day<sup>-1</sup> m<sup>-1</sup>, and dissolved organic nitrogen (DON) = 0.08–0.09 mol day<sup>-1</sup> m<sup>-1</sup>;

- 5) electrical resistivity surveys (marine CRP and land-based, stationary) were used to examine the movement of the fresh water/salt water interface in response to the lunar tide, as well as to map the offshore extent of the SGD zone. The land-based, tidal resistivity surveys were used to delineate the zone of active SGD (50 m).

#### Acknowledgments

This work could not have been accomplished without the expert help of many, including Chris Reich (USGS–St. Petersburg, FL), Marci Marot (USGS–St. Petersburg, FL), and Jason Greenwood (ETI, Inc.). PWS especially thanks John Haines for continued support thorough the USGS Coastal and Marine Geology (CM&G) Program and the City of Santa Barbara, which partially funded this project cooperatively with the USGS Water Resources Division. PWS thanks Jon Warrick (USGS–Santa Cruz, CA), John Bratton (USGS–Woods Hole, MA) and three anonymous reviewers for their expert critique of an earlier draft of the paper, and Eric Wolanski (AIMS) for editorial handling. The use of trade names is for descriptive purposes only and does not imply endorsement by the U.S. Government.

#### References

- Beighley, R.E., Dunne, T., Melack, J.M., 2008. Impacts of climate variability and land use alterations on frequency disruptions of terrestrial runoff loadings to coastal waters in southern California. *Journal of the American Water Resources Association* 44, 62–74.
- Boehm, A.B., 2007. Enterococci concentrations in diverse coastal environments exhibit extreme variability. *Environmental Science and Technology* 41, 8227–8232.
- Boehm, A.B., Weisberg, S.B., 2005. Tidal forcing of enterococci at fortnightly and semi-diurnal frequencies. *Environmental Science and Technology* 39, 5575–5583.
- Boehm, A.B., Shellenbarger, G.G., Paytan, A., 2004. Groundwater discharge: potential association with fecal indicator bacteria in the surf zone. *Environmental Science and Technology* 38, 3558–3566.
- Boehm, A.B., Paytan, A., Shellenbarger, G.G., Davis, K.A., 2006. Composition and flux of groundwater from a California beach aquifer: implications for nutrient supply to the surf zone. *Continental Shelf Research* 26, 269–282.
- Burnett, W.C., Dulaiova, H., 2003. Estimating the dynamics of groundwater input into the coastal zone via continuous radon-222 measurements. *Journal of Environmental Radioactivity* 69, 21–35.
- Burnett, W.C., Kim, G., Lane-Smith, D., 2001. A continuous radon monitor for assessment of radon in coastal ocean waters. *Journal of Radioanalytical and Nuclear Chemistry* 249, 167–172.
- Burnett, W.C., Chanton, J., Christoff, J., Kontar, E., Krupa, S., Lambert, M., Moore, W., O'Rourke, D., Paulsen, R., Smith, C., Smith, L., Taniguchi, M., 2002. Assessing methodologies for measuring groundwater discharge to the ocean. *EOS* 83, 117–123.
- Burnett, W.C., Cable, J.E., Corbett, D.R., 2003. Radon tracing of submarine groundwater discharge in coastal environments. In: Taniguchi, M., Wang, K., Gamito, T. (Eds.), *Land and Marine Hydrogeology*. Elsevier Publications, pp. 25–43.
- Burnett, W.C., Aggarwal, P.K., Bokuniewicz, H., Cable, J.E., Charette, M.A., et al., 2006. Quantifying submarine groundwater discharge in the coastal zone via multiple methods. *Science of the Total Environment* 367, 498–543.
- Burnett, W.C., Santos, I., Weinstein, Y., Swarzenski, P.W., Herut, B., 2007. Remaining uncertainties in the use of Rn-222 as a quantitative tracer of submarine groundwater discharge. In: Sanford, W., Langevin, C., Polemio, M., Povinec, P. (Eds.), *A New Focus on Groundwater–Seawater Interactions*, 312. IAHS Publ, pp. 109–118.
- Burnett, W.C., Peterson, R., Moore, W.S., Oliveira, J., 2008. Radon and radium isotopes as tracers of submarine discharge – results from the Ubatuba, Brazil SGD assessment inter-comparison. *Estuarine Coastal Shelf Science* 76, 501–511.

- Capone, D.G., Bautista, M.F., 1985. A groundwater source of nitrate in nearshore marine sediments. *Nature* 313, 214–216.
- Charette, M.A., Buesseler, K.O., 2004. Submarine groundwater discharge of nutrients and copper to an urban subestuary of Chesapeake Bay (Elizabeth River). *Limnology and Oceanography* 49, 376–385.
- Charette, M.A., Sholkovitz, E.R., 2006. Trace element cycling in a subterranean estuary: Part 2. Geochemistry of the pore water. *Geochimica et Cosmochimica Acta* 70, 811–826.
- Charette, M.A., Buesseler, K.O., Andrews, J.E., 2001. Utility of radium isotopes for evaluating the input and transport of groundwater-derived nitrogen to a Cape Cod estuary. *Limnology and Oceanography* 46, 465–470.
- Charette, M.A., Moore, W.S., Burnett, W.C., 2008. Uranium- and thorium-series nuclides as tracers of submarine groundwater discharge. In: Krishnaswami, S., Cochran, J.K. (Eds.), *Radioactivity in the Environment*, vol: "U-Th Series Nuclides in Aquatic Systems", 13, pp. 155–191.
- Colbert, S.L., Hammond, D.E., 2007a. Temporal and spatial variability of radium in the coastal ocean and its impact on computation of nearshore cross-shelf mixing rates. *Continental Shelf Research* 27, 1477–1500.
- Colbert, S.L., Hammond, D.E., 2007b. Shoreline and seafloor fluxes of water and short-lived Ra isotopes to surface water of San Pedro Bay, CA. *Marine Chemistry* 108, 1–17.
- Colbert, S.L., Hammond, D.E., Berelson, W.M., 2008a. Radon-222 budget in Catalina Harbor, California: 1. Water mixing rates. *Limnology and Oceanography* 53, 651–658.
- Colbert, S.L., Berelson, W.M., Hammond, D.E., 2008b. Radon-222 budget in Catalina Harbor, California: 2. Flow dynamics and residence time in a tidal beach. *Limnology and Oceanography* 53, 659–665.
- Dulaiova, H., Burnett, W.C., 2004. An efficient method for gamma spectrometric determination of  $^{226,228}\text{Ra}$  via Mn fibers. *Limnology and Oceanography*, Methods 2, 256–261.
- Dulaiova, H., Burnett, W.C., 2006. Radon loss across the water/air interface estimated from  $^{222}\text{Rn}/^{224}\text{Ra}$ . *Geophysical Research Letters* 33, L05606. doi:10.1029/2005GL025023.
- Dulaiova, H., Peterson, R., Burnett, W.C., Lane-Smith, D., 2005. A multidetector continuous monitor for assessment of  $^{222}\text{Rn}$  in the coastal ocean. *Journal of Radioanalytical and Nuclear Chemistry* 263 (2), 361–365.
- Dulaiova, H., Burnett, W.C., Chanton, J.P., Moore, W.S., Bokuniewicz, H.J., Charette, M.A., Sholkovitz, E., 2006a. Assessment of groundwater discharges into West Neck Bay, New York, via natural tracers. *Continental Shelf Research* 26, 1971–1983.
- Dulaiova, H., Burnett, W.C., Wattayakorn, G., Sojisuporn, P., 2006b. Are groundwater inputs into river-dominated areas important? The Chao Phraya River – Gulf of Thailand. *Limnology and Oceanography* 51, 2232–2247.
- Freckleton, J.R., Martin, P., Nishikawa, T., 1998. Geohydrology of Storage Unit III and a Combined Flow Model of the Santa Barbara and Foothill Ground-water Basins, Santa Barbara County, California. U.S. Geological Survey Water-Resources Investigations Report 97-4121, pp. 85.
- Izbicki, J.A., Swarzenski, P.W., Reich, C., Rollins, C., Holden, P., in review. Sources of fecal indicator bacteria in urban streams and ocean beaches, Santa Barbara, CA. Water Research.
- Macintyre, S., Wanninkhof, R., Chanton, J.P., 1995. Trace gas exchange across the air/sea interface in freshwater and coastal marine environments. In: Matson, P.A., Harris, R.C. (Eds.), *Biogenic Trace Gases: Measuring Emissions from Soil and Water*. Blackwell Science Ltd., pp. 52–97.
- Manheim, F.T., Krantz, D.E., Bratton, J.F., 2004. Studying groundwater under DELMARVA coastal bays using electrical resistivity. *Groundwater* 42, 1052–1068.
- Martin, P., 1984. Ground-water Monitoring at Santa Barbara, California: Phase 2-Effects of Pumping on Water Levels and on Water Quality in the Santa Barbara Ground-Water Basin. U.S. Geological Survey Water-Supply Paper 2197, pp. 36.
- McFadden, M.C., Polinoski, K.G., Martin, P., 1991. Measurement of Streamflow Gains and Losses on Mission Creek at Santa Barbara, California, July and September, 1987. U.S. Geological Survey Water Resources-Investigations Report 91-4002, 15 p. <http://pubs.er.usgs.gov/usgspubs/wri/wri914002>.
- McFee-Shaw, E.E., Siegel, D.A., Washburn, L., Brzezinski, M.A., Jones, J.L., Leydecker, A., Melack, J., 2007. Mechanisms for nutrient delivery to the inner shelf: observations from the Santa Barbara channel. *Limnology and Oceanography* 52, 1748–1766.
- Michael, H.A., Mulligan, A.E., Harvey, C.F., 2005. Seasonal oscillations in water exchange between aquifers and the coastal ocean. *Nature* 436, 1145–1148.
- Moore, W.S., 1996. Large groundwater inputs to coastal waters revealed by  $^{226}\text{Ra}$  enrichments. *Nature* 380, 612–614.
- Moore, W.S., 2000a. Determining coastal mixing rates using radium isotopes. *Continental Shelf Research* 20, 1995–2007.
- Moore, W.S., 2000b. Ages of continental shelf waters determined from  $^{223}\text{Ra}$  and  $^{224}\text{Ra}$ . *Journal of Geophysical Research* 105, 22117–22122.
- Moore, W.S., 2006. The role of submarine groundwater discharge in coastal biogeochemistry. *Journal of Geochemical Exploration* 88, 389–393.
- Moore, W.S., Arnold, R., 1996. Measurement of  $^{223}\text{Ra}$  and  $^{224}\text{Ra}$  in coastal waters using a delayed coincidence counter. *Journal of Geophysical Research* 101, 1321–1329.
- Moore, W.S., de Oliveira, J., 2008. Determination of residence time and mixing processes of the Ubatuba, Brazil, inner shelf waters using natural Ra isotopes. *Estuarine, Coastal and Shelf Science* 76 (3), 512–521.
- Muir, K.S. 1968. Ground-water Reconnaissance of the Santa Barbara-Montecito Area, Santa Barbara County, California. U.S. Geological Survey Water-Supply Paper 1859-A., pp. 36.
- Mulligan, A.E., Charette, M.A., 2006. Inter-comparison of submarine groundwater discharge estimates from a sandy unconfined aquifer. *Journal of Hydrology* 327, 411–425.
- Paytan, A., Boehm, A.G., Shellenbarger, G.G., 2004. Bacterial contamination and submarine groundwater discharge—a possible link. *Environmental Chemistry* 1, 29–30.
- Robinson, C., Li, L., Barry, D.A., 2007a. Effect of tidal forcing on a subterranean estuary. *Advances in Water Resources* 30, 851–865.
- Robinson, C., Li, L., Prommer, H., 2007b. Tide induced recirculation across the aquifer-ocean interface. *Water Resources Research* 43, W07428. doi:10.1029/2006WR005679.
- Rosenberry, D.O., Morin, R.H., 2004. Use of an electromagnetic seepage meter to investigate temporal variability in lake seepage. *Groundwater* 42, 68–77.
- Swarzenski, P.W., Reich, C.D., Spechler, R.M., Kindinger, J.L., Moore, W.S., 2001. Using multiple geochemical tracers to characterize the hydrogeology of the submarine spring off Crescent Beach, Florida. *Chemical Geology* 179, 187–202.
- Swarzenski, P.W., 2007. U/Th series radionuclides as tracers of coastal groundwater. *Chemical Reviews* 107 (2), 663–674. doi:10.1021/cr0503761.
- Swarzenski, P.W., Baskaran, M., 2007. Uranium distribution in the coastal waters and pore waters of Tampa Bay, Florida. *Marine Chemistry* 104, 43–57.
- Swarzenski, P.W., Charette, M., Langevin, C., 2004. An Autonomous, Electromagnetic Seepage Meter to Study Coastal Groundwater/Surface Water Exchange. U.S. Geological Survey OFR 2004-1369.
- Swarzenski, P.W., Burnett, W.C., Weinstein, Y., Greenwood, W.J., Herut, B., Peterson, R., Dimova, N., 2006a. Combined time-series resistivity and geochemical tracer techniques to examine submarine groundwater discharge at Dor Beach Israel. *Geophysical Research Letters* 33, L24405. doi:10.1029/2006GL028282.
- Swarzenski, P.W., Orem, W.G., McPherson, B.F., Baskaran, M., Wan, Y., 2006b. Biogeochemical transport in the Loxahatchee river estuary: the role of submarine groundwater discharge. *Marine Chemistry* 101, 248–265.
- Swarzenski, P.W., Simonds, F.W., Paulson, T., Kruse, S., Reich, C., 2007a. A geochemical and geophysical examination of submarine groundwater discharge and associated nutrient loading estimates into Lynch Cove, Hood Canal, WA. *Environmental Science and Technology* 41, 7022–7029.
- Swarzenski, P.W., Kruse, S., Reich, C., Swarzenski, W.V., 2007b. Multi-channel resistivity investigations of the fresh water/saltwater interface: a new tool to study an old problem. In: Sanford, W., Langevin, C., Polemio, M., Povinec, P. (Eds.), *A New Focus on Groundwater-Seawater Interactions*, 312. IAHS Publ, pp. 100–108.
- Swarzenski, P.W., Reich, C., Kroeger, K., Baskaran, M., 2007c. Ra and Rn isotopes as natural tracers of submarine groundwater discharge in Tampa Bay, FL. *Marine Chemistry* 104, 69–84.
- Taniguchi, M., 2002. Tidal effects on submarine groundwater discharge into the ocean. *Geophysical Research Letters* 29. doi:10.1029/2002GL014987.
- Taniguchi, M., Fukuo, Y., 1993. Continuous measurements of ground-water seepage using an automatic seepage meter. *Groundwater* 31, 675–679.
- Taniguchi, M., Burnett, W.C., Smith, C.F., Paulsen, R.J., O'Rourke, D., Krupa, S.L., Christoff, J.L., 2003. Spatial and temporal distributions of submarine groundwater discharge rates obtained from various types of seepage meters at a site in the Northeastern Gulf of Mexico. *Biogeochemistry* 66, 35–53.
- Taniguchi, M., Ishitobi, T., Burnett, W.C., Wattayakorn, G., 2007. Evaluating groundwater – sea water interactions via resistivity and seepage meters. *Groundwater* 45, 729–735.
- Warrick, J.A., Washburn, L., Brzezinski, M.A., Siegel, D.A., 2005. Nutrient contributions to the Santa Barbara Channel, California, from the ephemeral Santa Clara River. *Estuarine Coastal and Shelf Science* 62, 559–574.
- Weinstein, Y., Burnett, W.C., Swarzenski, P.W., Shalem, Y., Yechieli, Y., Herut, B., 2007. Fresh groundwater discharge and seawater recycling – the role of aquifer heterogeneity: an example from the Carmel coast, Israel. *Journal of Geophysical Research* 112, C12016. doi:10.1029/2007J0004112.
- Yamahara, K.M., Layton, B.A., Santoro, A.E., Boehm, A.B., 2007. Beach sands along the California coast are diffuse sources of fecal bacteria to coastal waters. *Environmental Science and Technology* 41, 4515–4521.